E-ISSN 2586-9027
Homepage : *https://tci-thaijo.org/index.php/SciTechAsia* Science & Technology Asia
Vol.30 No.4 October - December 2025 Page: [244-259]

Original research article

Numerical And Experimental Study On Shear Strength Of High Strength Reinforced Concrete

Cherukupally Rajesh[1], Vaddemani Guru Prathap Reddy[2,*]

[1] *Department of Civil Engineering, Prasad V. Potluri Siddhartha Institute of Technology (PVPSIT), Vijayawada 520007, India*
[2] *Department of Civil Engineering, National Institute of Technology (NIT) Nagaland 797103, India*

Received 22 April 2025; Received in revised form 16 January 2026
Accepted 19 February 2026; Available online 17 December 2025

ABSTRACT

Shear strength of concrete is a vital consideration in the analysis and design of structures, as its failure occurs abruptly and can result in catastrophic consequences. In the current study, two different grades of reinforced concrete beams were examined, each with three shear span-to-depth ratios (a/d) of 1, 2, and 3. The beams were both cast and experimentally tested. Additionally, numerical simulations of the beams were conducted using the ATENA software to model and analyze their performance. In ATENA, the material for concrete was assigned using the cementitious2 and cementitious2-user models. The cementitious2 model includes the Euro-Code and Model-Code as default models, both of which were utilized in the study to determine the shear strength of reinforced concrete beams. For the Cementitious2user material model, the compressive stress-strain model can be user-defined. In this study, the GRK stress-strain model and Mander's stress-strain model were used as input to calculate the shear strength of the reinforced concrete beams. The results showed that the shear strength of the test specimens increased with the concrete strength for all a/d ratios. However, as the a/d ratio increased from 1 to 3, the shear strength decreased by approximately 60%. The shear strength values obtained using ATENA with various models were compared with the experimental results, and it was found that the shear strength behavior from the numerical simulations closely matched the experimental results.

Keywords: High strength concrete; Numerical modelling; Reinforced concrete; Shear strength

***Corresponding author:** vguruprathap@gmail.com
doi: xx.xxxxx/scitechasia.xxxx.xx

1. Introduction

The evaluation of shear strength in High Strength Reinforced Concrete (HSRC) beams with the stirrups is crucial for ensuring the structural integrity and performance of concrete structures. Various studies have identified multiple factors, such as spacing of stirrups, dimensions of beams, and properties of materials, which significantly influence shear strength.

Recently, numerical analysis, particularly the use of finite element software like ATENA, has been playing a pivotal role in simulating the behavior of Reinforced Concrete (RC) beams under shear loading.

The experiments on the shear behavior of Ultra High Performance Concrete (UHPC) beams highlighted the limited scope of numerical research, which indicates the need for comprehensive studies [1]. UHPC beams can be compared to HSRC beams due to similarities in mechanical properties. These advanced modeling techniques not only assist in predicting shear strength but also aid in refining design methodologies. The research on changes in behaviour of deep beams which were reinforced with Glass Fiber Reinforced Polymer (GFRP) bars, illustrated the importance of selection of material on shear performance [2].

Studies on machine learning have demonstrated the uses of Support Vector Regression (SVR) in predicting shear strength based on different geometric and parameters of material, and reaffirming the complexity of deriving shear strength [3]. This innovative methodology suggests that numerical models can be enhanced with data-driven techniques, potentially increasing prediction accuracy for HSRC beams reinforced with stirrups. Moreover, empirical investigations have provided data on the shear strength of recycled self-compacted concrete deep beams, demonstrating how the stirrups significantly affect the shear behaviour[4]. The findings of experimental evaluations on the shear behaviour of concrete deep beams reinforced with CFRP, GFRP, provides insight into how various materials and reinforcement configurations influence performance [5].

The performance of HSRC beams, particularly under varying loading conditions and shear span-to-depth ratios (a/d ratios), is critical. The shear behaviour in beams with hybrid fiber reinforcement shows that the increase in reinforcement can improve shear capacities [6]. The above findings align with a developed shear strength model which effectively predicts the shear strength of reinforced concrete (RC) beams with stirrups [7]. RC beam shear strength depends on some crucial parameters such as concrete compressive strength, longitudinal reinforcement ratio and size of stirrup.

Overall it can be said that the numerical and experimental studies highlighted the significance of a multi-factorial approach in evaluating the shear strength of HSRC beams with stirrups. Implementing the advanced numerical modelling, supported by machine learning techniques and experimental validation, offers a comprehensive approach for engineers who are aiming to optimize shear design in Reinforced Concrete (RC) structures.

The compressive strength of High Strength Concrete (HSC) typically ranges from 50 MPa to 100 MPa. Compared to Normal Strength Concrete (NSC), HSC has advantages in terms of compressive strength, stiffness, and durability. These advantages have lead to its increased use over the past few decades [8-9]. HSC also improves the shear strength of concrete [10-12]. However, in HSC, the paste strength is higher than that of aggregates, so, when a concrete member fails in shear, cracks propagate through the aggregates, leading to smoother failure surfaces [13, 14].

The shear strength of structural members is primarily determined by the balance between the compression field and the contribution of shear reinforcement, such as stirrups or alternative lateral confinement systems. Present design codes of concrete define shear strength contributions for members with and without shear reinforcement. Research studies on the shear strength of plain concrete members typically focus on beams with strong compression zones, subjected to high bending moments and shear loads. While

these studies have significantly advanced our understanding of shear strength in plain members, they offer limited insights into the direct shear contribution of concrete, since these failures often involve the action of combined stress conditions.

A critical review of research on RC beams highlights the importance of experimental investigations in quantifying the shear strength provided by the concrete portion alone. Research conducted in the 1980s found that an increase in beam size led to a decrease in the "ratio of inner stirrup tensile strain to yield strain" [15]. Research was also carried out on the influence of the shear span-to-depth ratio (a/d) on failure modes of concrete beams [16, 17]. Beams with an a/d ratio below 1.0 exhibit deep beam failure, while those with an a/d ratio between 1.0 and 2.5 undergo shear compression failure. Beams with an a/d ratio between 2.5 and 6.0 experience shear tension failure, and those with an a/d ratio above 6.0 typically fail in flexure [18-19]. In reinforced concrete beams subjected to four-point loading, when the loading point is near the support, the failure was shear failure, whereas flexural failure becomes predominant as the loading point moves toward the mid-span [20, 21].

Additionally, research on the spacing of stirrups and shear reinforcement has shown that shear strength increases as spacing of stirrups decreases [22, 23]. However, despite the increased compressive strength of HSC, its ability to resist shear failure is limited due to increased brittleness caused by a strengthened paste phase. Studies on the shear strength of HSC beams have considered factors such as size effects, the presence of web reinforcement, and the percentage of longitudinal reinforcement [24-25].

In the present study, the shear strength of HSC reinforced concrete beams is investigated, considering size effects and the influence of web reinforcement. Additionally, numerical analyses of the experimental beams are conducted using ATENA software. The GRK model [26] and Mander's model [27] are used for compression modelling. Default models available in ATENA, such as the Eurocode (EC) and Model Code (MC), are also considered to evaluate the shear strength of HSC reinforced concrete beams.

2. Experimental Work

The experimental investigation consists of casting and testing two series of beams, D and F. Each series consists of three beams. All beams had rectangular cross-sections of overall dimensions of 100mm wide, 200mm deep and 2000mm long. The dimensions and details of beams are shown in Figs. 1-2. The compression steel in the six beams was 2no.s 8mm diameter, and tension steel was 2no.s 12 mm diameter for Series-D and 2no.s 16mm diameter for Series-F. The shear reinforcement was designed for these beams. The shear reinforcement provided was halved to ensure that the beam fails in shear mode.

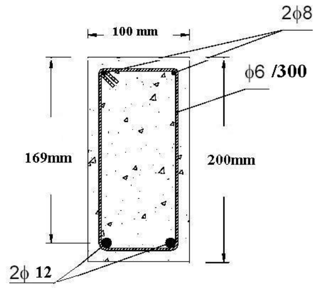

Fig. 1. Cross-section details for specimens Dad1, Dad2 and Dad3.

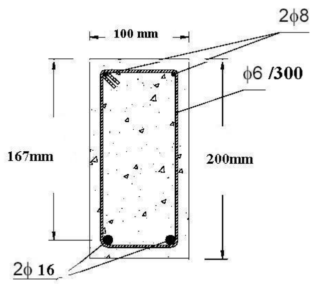

Fig. 2. Cross-section details for specimens Fad1, Fad2, and Fad3.

2.1 Material properties & Mix proportions

In the current project, Portland Pozzolana Cement (PPC) of grade 53, complying with IS 1489:1991 (Reaffirmed 2005) [28], was utilised. Fine aggregate sourced from local river sand, conforming to Zone II as per IS 383-2016 [29], was used in this investigation. Crushed granite stone, obtained from a nearby crusher, was employed as the coarse aggregate, with

sizes ranging from 20 mm to 4.75 mm, and conforming to IS 383-2016 [29]. The specific gravity of the cement was 3.15, while the specific gravity of the fine aggregate was 2.56, and that of the coarse aggregate was 2.80. Concrete mix proportions for seven different strengths were designed using the IS 10262-2019 [30] method of mix design. The final mix proportions were determined based on trial mixes conducted in the laboratory. A Poly Carboxylic Ether (PCE) based chemical admixture, branded as CHRYSO OPTIMA K9313, was used to enhance the workability of concrete with compressive strengths of 50 MPa and 70 MPa. After casting, the specimens were kept under moist conditions and immersed in a curing pond after 24 hours. The samples remained in the pond for 28 days for curing. Following the curing regime, the samples were removed from the pond and stored indoors before testing. Table 1 presents the concrete mix proportions for series D and F.

Table 1. Materials specifications.

Materials	Series-D	Series-F
Mix Proportions	1:1.22:2.27	1:0.55:1.1
Cement in kg/m^3	457	836.7
Coarse aggregate in kg/m^3	1234	920.4
Fine aggregate in kg/m^3	558	460.2
Water in L/m^3	196.51	225.9
Super-plasticizer in L/m^3	——	12.55
Water cement ratio	0.43	0.27
Air Content (%)	1.69	1.17
Slump value mm	85	77
Cube compressive strength (MPa)	53.86	72.17
Standard Deviation	0.48	0.35

2.1.1 Torsteel

Torsteel bars of 8mm, 12mm and 16mm nominal diameters are used. Three samples of 450mm for each diameter were taken for tension tests. These were tested on U.T.M of 20 tones capacity. A Tinius-Olsen extensometer of 200mm gauge length with a least count of 0.002mm was used to measure elongations. The stresses and corresponding strains were plotted for all three samples of each bar on one sheet and the average yield stress value was considered. The yield stress values for three bars (8, 12 and 16mm bars) are 450N/mm^2, 494N/mm^2 and 470N/mm^2, respectively.

2.1.2 Mild steel

Mild steel of 6mm diameter was used for ties. Three samples were tested for mechanical properties; the yield stress of 6mm diameter mild steel bar was 254 N/mm^2. The stress-strain curves of various diameters of steel were placed in Appendix A for reference.

Table 2. Spacing and percentage web reinforcement of two series of beams Specimen Label Compressive strength of concrete (f_c).

Specimen Label	Compressive strength of concrete (f_c) (MPa)	a/d ratio	ρ_w	Stirrups spacing (mm)
Dad1	53.86	1	1.34	300
Dad2	56.98	2	1.34	300
Dad3	53.86	3	1.34	300
Fad1	72.67	1	2.41	300
Fad2	71.67	2	2.41	300
Fad3	72.34	3	2.41	300

2.2 Preparation of test specimens

The reinforcement cage consists of 2-8mm diameter for compression and 2-12mm diameter; 2-16mm diameter bars as tension reinforcement for series D and F, respectively. Steel bars of required length were cut and straightened. 6mm diameter mils steel bars were cut to the required length and bent to form stirrups. The stirrups were tied to the longitudinal bars such that the hooks are staggered on either side.

In order to provide the necessary cover, the reinforcing cages were inserted in the steel moulds. The cage was positioned on cover blocks to achieve this. Before insertion of the cage into position, a lubricant was applied to the steel moulds. Three layers of concrete were poured in the mould and each layer was compacted using a 25 mm diameter electrically powered needle vibrator running at a speed of 2850 rpm. The concrete was mixed in separate batches in an electrically powered mixer. To level the top surface, a plate vibrator was used to vibrate the top layer of concrete. Mould bulging was prevented by the application of clamps.

After casting, the moulds were taken out the next day. The curing tank was filled with named beams and supporting specimens. The beam specimens were allowed to cure for up to 28 days after which they were white washed to make it easier to see cracking patterns during testing and stored in a cool, dry area until they were tested.

2.3 Experimental testing procedure

Using the Tinius-Olsen testing machine, all those beams were investigated. With a minimum count of 100 lbs. and 1000 lbs., the machine has two loading ranges of 60,000 lbs. and 400 000 lbs. A steel I-section beam, as illustrated in Fig. 3, was used to apply a two-point symmetrical load. On the machine cross heads, the test beams were positioned such that they were centred over the supports. On the experimental beams, load points have been marked with the required a/d ratios. A two-point load test was performed on the beams. At the span's centre and the two load points that had previously been marked, deflection gauges with a minimum count of 0.01mm and a range of 50mm were fixed. The cross-head of the machine was lifted until the fixed head of the machine just touched the roller located in the middle of the loading beam.

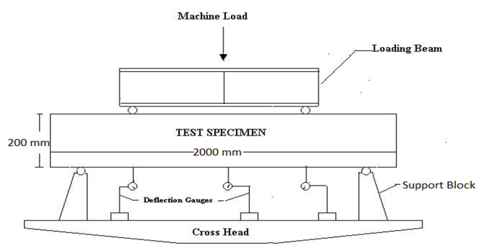

Fig. 3. Experimental setup.

2.4 ATENA modelling & testing procedure

There were many material models present in ATENA to assign material properties such as solid elastic, solid steel, solid concrete, 1D reinforcement, etc. The solid concrete was further classified into various categories cementitious2, cementitious2user, cementitious2 SHCC HPFRC, cementitious2 variable, cementitious3, Reinforced concrete, SBETA material, etc. In ATENA, concrete was modeled using the Cementitious2, which is a nonlinear fracture–plastic constitutive model. The Eurocode (EC) and Model Code (MC) are built-in formulations available within the Cementitious2 framework. These two were adopted to estimate shear strength parameters. In addition, the Cementitious2-User option was also employed to incorporate user-defined compressive stress–strain relationships based on the GRK model [26] and Mander's model [27]. This is done to enable a comparative assessment of confined concrete behavior in reinforced concrete beams. Although the GRK and Mander models were originally developed for confined concrete in columns, they were employed in the present study to examine whether their compressive stress–strain formulations could realistically represent concrete behavior in shear-critical beam elements. Their use does not imply direct applicability to beams but enables a comparative numerical evaluation.

The reinforcement was modelled as 1D reinforcement in ATENA and the properties of the reinforcement were taken as the yield strength values for three bars (8, 12 and 16mm bars) was 500 MPa and 6 mm stirrup was 250 MPa. The loading plate and support plate was given as Solid Elastic material with an elastic modulus of 2×105 MPa. The reinforced concrete beam modelled in ATENA software was a half of beam cast and tested experimentally as it is symmetric. The rollers at supports and loading points are taken as rectangular beams because rollers have a line contact with the surface of the beam. In ATENA there is a difficulty in fixing the contact surface of loading roller and beam surface. The fixed contact can be achieved between surface to surface and the fixed contact cannot be achieved in between line and surface, therefore in place of rollers rectangular beams of size 100 mm × 100 mm × 50 mm are considered. Fig. 4 shows the modelled beam in ATENA before constraints, after constraints, and after assigning materials. A mesh sensitivity analysis was first carried out, on a reinforced concrete beam of same size and similar grade which acted as a representative beam, to identify a mesh size that ensured numerical convergence with acceptable computational cost. Since all beam specimens had identical geometry and reinforcement detailing, the same finalized mesh size of 5 mm was adopted for all numerical models. The convergence results of the mesh sensitivity study are presented in Appendix B.

Two types of meshes were used in this model: one was structured mesh and the other was unstructured mesh. The structured mesh was considered for the concrete beam and the mesh was taken in such a way that the size of the mesh was equal to 5mm after mesh sensitivity analysis. The unstructured mesh was considered for beam elements, where the mesh is directly taken. The elements such as Hexahedra and Tetrahedra, were present in the meshing options. The Hexahedra was given to structured mesh, and the Tetrahedra was given to unstructured mesh types. This was suggested by the ATENA software. The mesh image of a beam is shown in Fig. 5

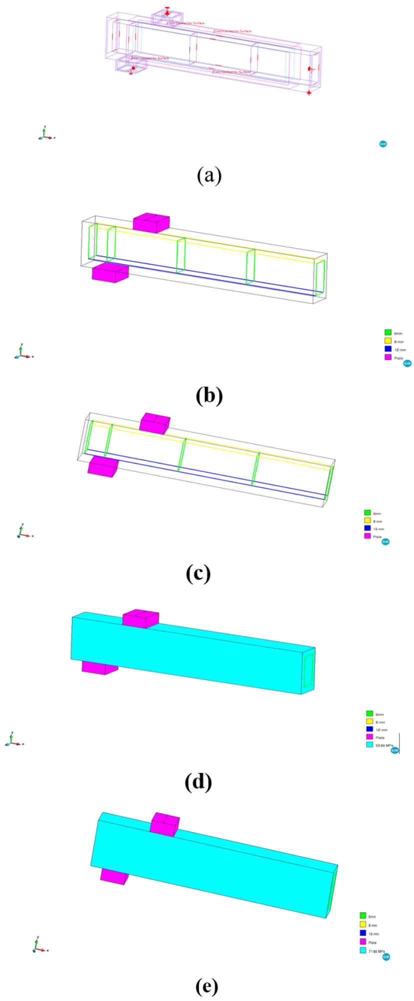

Fig. 4. Beam modelling in ATENA (a) Beam with constraints and monitor points (b) & (c) Beam showing the assigned material for reinforcement for Dad1 beam and Fad1 beam respectively (d) & (e) Dad1 & Fad1 beams assigned with concrete respectively.

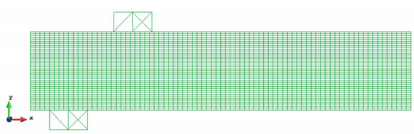

Fig. 5. Beam with mesh size of 5 mm.

The loading was applied at the top center of the loading plate and a monitor for load was considered at the same point. The monitors for deflection were considered at loading point and also at the center of the beam.

3. Results and Discussions

Table 3 shows the results of the six tests of beam specimens subjected to shear.

The load deflection curves at three points, namely mid-span and two points under the loads, for each were drawn on a single sheet. In all beams, central deflections were greater than deflections at other points, and deflection curves at load points were nearly similar for all beams. The higher deflections observed at mid-span are attributed to the maximum bending moment occurring at the beam center under symmetric two-point loading. Deflections at the load application points were comparatively lower and exhibited similar trends across all specimens due to identical loading configurations and boundary conditions. The load deflection curves for various beam specimens are shown in Figs. 6(a)-(b).

There were no cracks in any of the beam specimens until 20% to 25% of the maximum load, when they all collapsed in shear. Till tension cracks developed, all beams behaved linearly. The bottom of the beams witnessed the beginning of tension cracks, which then grew vertically upward. As the load increased, new cracks began to form between the supports and the closest load points around 40% to 50% of the ultimate load. As the load climbed, these cracks curved towards the point of loading as shown in Figs. 7-8. Cracks began to appear in the pure moment zone during the early stages. These cracks first spread upward before the slanted crack began. Flexure cracks stopped spreading when the inclined crack initially showed up, and the inclined cracks began to move towards the

Table 3. Cracking shear strength (V_{cr}) and Ultimate shear strength (V_u) for beams.

Specimen	Compressive strength (f_c) (MPa)	a/d ratio	ρ_w	Stirrup spacing (mm)	V_u (MPa)	V_{cr} (MPa)	V_u/V_{cr}
Dad1	53.86	1	1.338	300	4.93	3.54	1.39
Dad2	56.98	2	1.338	300	3.12	2.30	1.35
Dad3	53.86	3	1.338	300	1.422	1.38	1.03
Fad1	72.67	1	2.408	300	10.73	4.54	2.36
Fad2	71.67	2	2.408	300	4.05	2.76	1.47
Fad3	72.34	3	2.408	300	2.96	1.84	1.61

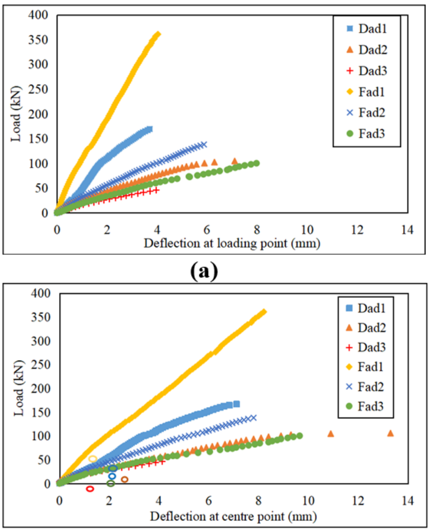

Fig. 6. (a) Load vs Deflection at loading point for Series-D and Series-F (b) Load vs Deflection at centre point for Series-D and Series-F, "O" indicates cracking load points.

top.

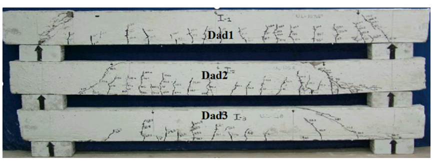

Fig. 7. Photographs of tested beams for Series-D.

The diagonal tension fractures started at or above the tension reinforcement in every beam and had an inclined orientation from where they began. The

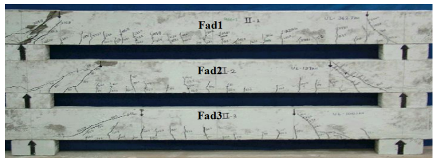

Fig. 8. Photographs of tested beams for Series-F.

diagonal stress fractures at both ends continued to grow as the loads began to rise. They often passed across the ends of the tension fractures at one end as they expanded towards the load point. At the opposite end, they either stretched along the tension reinforcement, causing horizontal splitting as illustrated in Figs. 7-8, or crossed the reinforcement at an angle between 30 and 60 degrees.

The beginning of the diagonal tension fracture was closer to the support in some of the beams (Dad1, Dad2). Table 3 provides the V_{cr} values for beam specimens' first diagonal tension cracking stresses. The failure of specimens with a/d value of 1 in both series (Dad1, Fad1) was identical. In these specimens, multiple inclined cracks developed at the point of loading, and with additional loading, these cracks came together and eventually, the concrete spalled off in that area. On each shear span for specimen Dad3, only one significant inclined crack formed.

3.1 Behaviour after formation of diagonal cracks

Table 3 displays the ratio of the ultimate load to the cracking load. For specimen Dad3, which failed suddenly, the cracking and ultimate loads were nearly equal, whereas for the remaining beams in both series, the ultimate load was greater than the cracking load. It is clear that, with the exception of specimen Dad3, all other specimens were able to withstand loads that were far greater than those responsible for the initial diagonal tension cracking. This error may be due to the defects of casting of the beam.

In most of the beams, a second major diagonal crack was formed parallel to the first crack either before or at failure. Between the two major cracks in beams Dad1 and Fad1, additional cracks were seen, causing a diagonal band of fractured concrete to extend from the support to the closest loading block. A second crack did not occur in beams Dad3 and Fad3.

Prior to failure, a residual compression zone of uncracked concrete existed between the diagonal crack tip and the compression face, allowing the continued transfer of compressive stresses. At ultimate load, crushing and spalling of concrete occurred in this compression zone which led to sudden loss of load-carrying capacity. This compression-controlled shear failure was clearly observed in beams Dad1 and Dad2.

3.2 Effect of concrete strength and a/d ratio on shear strength

3.2.1 Effect of concrete strength

In the present study, the shear strength of a beam was defined as the load corresponding to the formation of the first diagonal crack crossing the mid-depth of the beam. This is a criterion commonly adopted by several earlier researchers. The results indicate that, for all a/d ratios, shear strength increased with increasing concrete compressive strength, as shown in Fig. 8. This enhancement can be attributed to improved aggregate interlock, increased dowel action of longitudinal reinforcement, and higher load-carrying capacity of the compression zone in higher-strength concrete. The observed trend is in good agreement with findings reported in previous experimental investigations.

3.2.2 Effect of a/d ratio

Shear strength was reduced in each of the series as the a/d ratio increased. The impact of the a/d ratio on shear strength is shown in Fig. 8. The highest shear strength was observed in the beams having a/d ratio of 1, compared to other beams. The shear strength decreased by around 60% in both series when the a/d ratio changed from 1 to 3. Literature analysis reveals that the size impact was more apparent in HSC [30].

4. Validation of Numerical shear strength values with experimental results

Figs. 9-14 show the shear force (kN) vs Deflection (mm) of beams Dad1, Dad2, Dad3, Fad1, Fad2, Fad3 at both loading points and also at the centre point of the beam (Mid-span of beam), respectively. The Numerical results are obtained by using the Displacement control for all models. It can be observed from Figs. 9-14 that almost all the models used in Numerical based software ATENA were in line with the experimental results. Also, it was clearly observed that the deflections at the centre point of the beam were higher when compared with the loading point. It was clear from the figures that the shear forces are higher for beams with less shear span to depth ratio in both series of beams D and F. The shear forces are higher for series F beams for various shear span to depth ratios when compared with series D beams, as series F beams had more compressive strength and improved percentage tension reinforcement than series D beams. With the increase in a/d ratio from 1 to 3, the shear strength was found to reduce by about 60%.

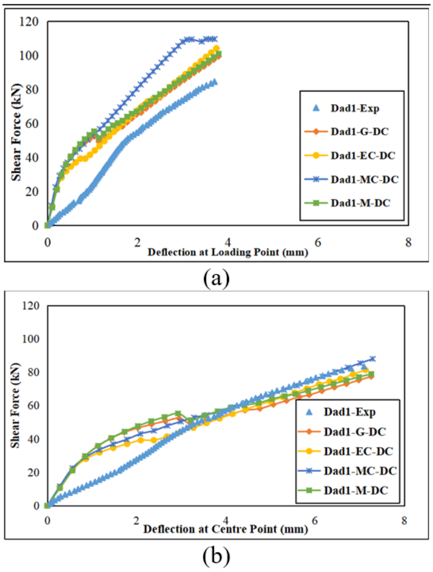

Fig. 9. Shear Force (kN) vs Deflection (mm) for Dad1 beam (a) at Loading Point (b) at Centre Point.

In Figs. 9-14; Dad1, Dad2, Dad3, Fad1, Fad2, Fad3 represent the beams; with D representing grade of concrete; ad the shear span to depth ratios, and 1, 2 and 3 the value of shear span to depth ratio. Exp represents experimental, G represents GRK Model, EC represents Euro Code, MC represents Model code, M represents Mander's code and DC represents displacement control.

Table 4 shows the comparison of shear strength values of experimental beams with numerical values using various

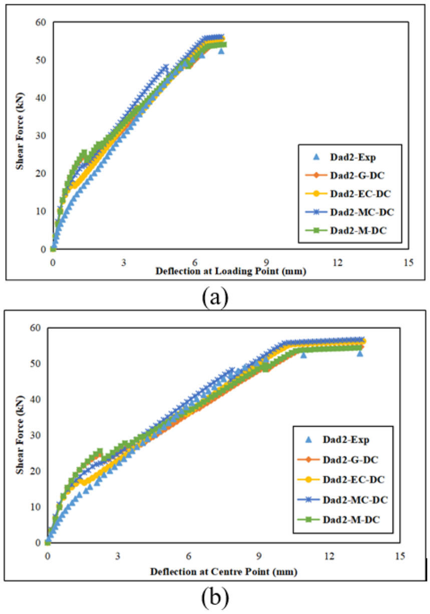

Fig. 10. Shear Force (kN) vs Deflection (mm) for Dad2 beam (a) at Loading Point (b) at Centre.

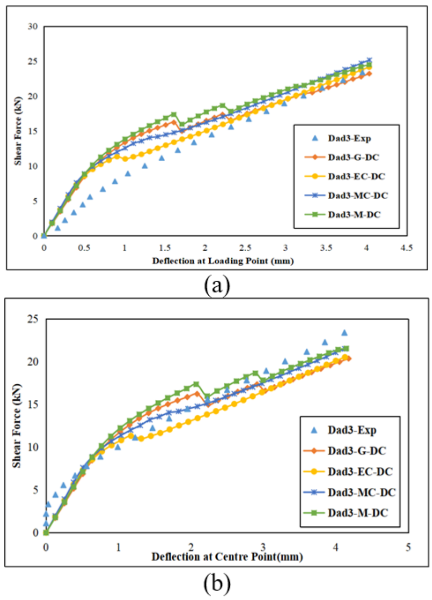

Fig. 11. Shear Force (kN) vs Deflection (mm) for Dad3 beam (a) at Loading Point (b) at Centre Point.

models. From the table, it is observed that the numerical shear strength values

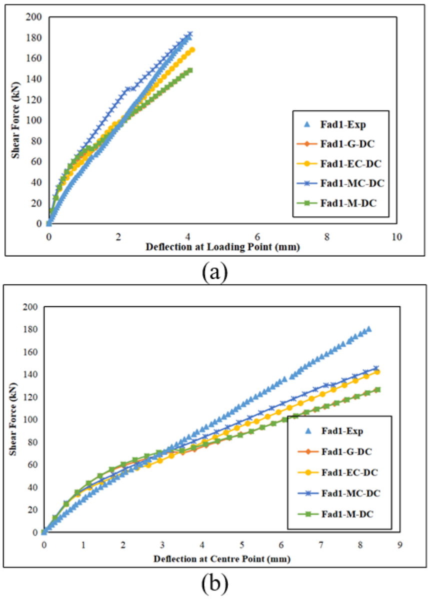

Fig. 12. Shear Force (kN) vs Deflection (mm) for Fad1 beam (a) at Loading Point (b) at Centre Point.

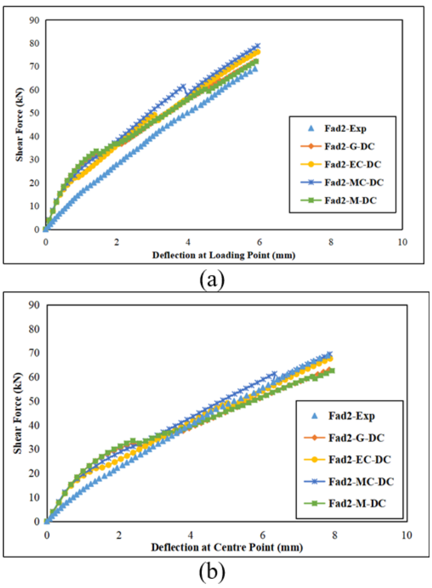

Fig. 13. Shear Force (kN) vs Deflection (mm) for Fad2 beam (a) at Loading Point (b) at Centre Point.

predicted by various models of Dad1 beam are higher than the experimental values

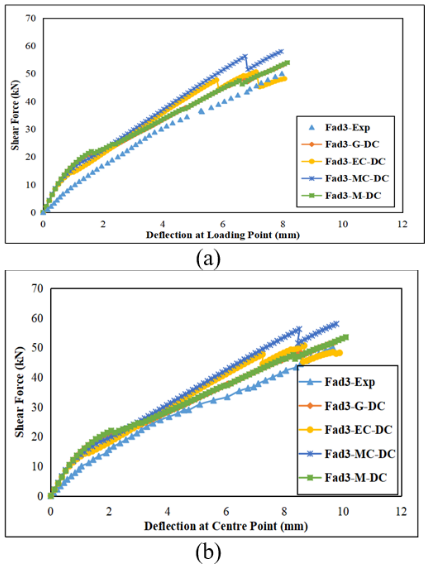

Fig. 14. Shear Force (kN) vs Deflection (mm) for Fad3 beam (a) at Loading Point (b) at Centre Point.

and lower than experimental for Fad1 beams. For other beams the prediction is almost within 10%. This variation may be due to some error in taking down the experimental values. But by considering all beams it can be clearly observed that the averages of predicted shear strengths of various models are similar to experimental shear strengths. The difference is 11% using Model code, within 5% for Euro Code, and within 2% for Mander's Model and GRK Model. Tables 5-6 show the comparison of deflection values of experimental beams at loading point and center point of beam with numerical values using various models respectively. It can be clearly observed from the table that almost all the models predicted similar deflections both at loading point and center point of beam compared to experimental deflections. So, from this observation it can be concluded that the Numerical studies can be further extended to predict the shear strength of HSC reinforced concrete beams with various parameters such as change in tension reinforcement, web reinforcement, etc., without the experimental study which saves material, man power and time.

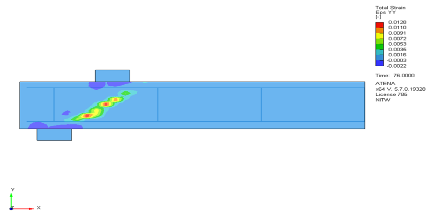

Fig. 15. Strains obtained using Numerical Analysis for Dad1 beam.

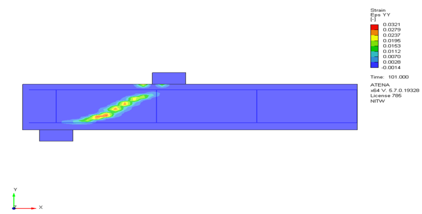

Fig. 16. Strains obtained using Numerical Analysis for Dad2 beam.

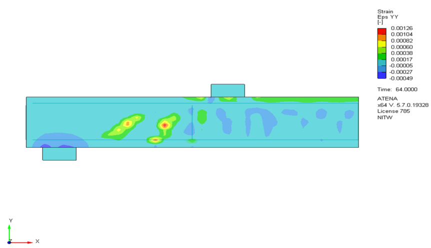

Fig. 17. Strains obtained using Numerical Analysis for Dad3 beam.

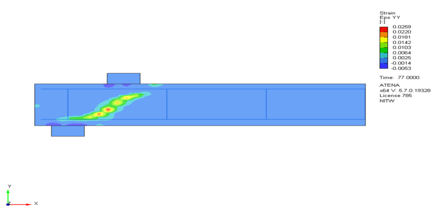

Fig. 18. Strains obtained using Numerical Analysis for Fad1 beam.

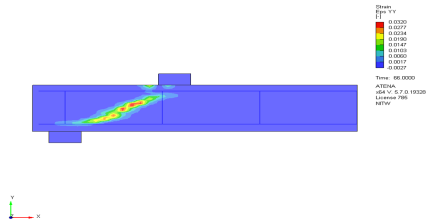

Fig. 19. Strains obtained using Numerical Analysis for Fad2 beam.

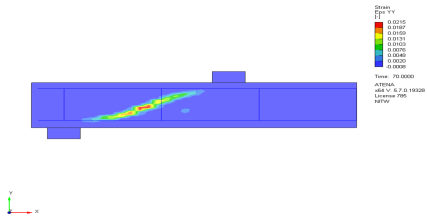

Fig. 20. Strains obtained using Numerical Analysis for Fad3 beam.

5. Conclusion

From the above experimental and numerical studies on shear strength of reinforced high-strength concrete beams, it can be concluded that:

1. In both the experimental and numerical studies, the shear strength of the test specimens increased as concrete strength increased for all a/d ratio values. This conforms to the findings of various other investigations.

2. As the shear span-to-depth ratio increased, the shear strength of the beams decreased. Shear strength is observed to decrease by around 60

3. Beams of both series were found to have an ultimate load that was significantly higher than the cracking load, except for Dad3 beam, which failed suddenly.

4. The Numerical shear strength values of various high-strength reinforced

Table 4. Comparison of shear strength (MPa) values of experiment with numerical.

Beam	a/d	Experimental shear strength (MPa)	ATENA shear strength results (MPa)				Experimental/ATENA results			
			Model code	Euro code	Mander's Model	GRK Model	Model code	Euro code	Mander's Model	GRK Model
Dad1	1	5.00	6.48	6.16	5.97	5.88	0.77	0.81	0.84	0.85
Dad2	2	3.10	3.32	3.29	3.20	3.20	0.93	0.94	0.97	0.97
Dad3	3	1.38	1.49	1.43	1.45	1.37	0.93	0.97	0.96	1.01
Fad1	1	10.66	10.86	9.95	8.78	8.78	0.98	1.07	1.21	1.22
Fad2	2	4.08	4.66	4.51	4.27	4.28	0.88	0.91	0.96	0.95
Fad3	3	2.96	3.43	2.85	3.19	3.16	0.86	1.04	0.93	0.94
						Average	0.89	0.96	0.98	0.99

Table 5. Comparison of experimental displacement (mm) values at Loading Point corresponding to peak load with numerical displacement (mm) values.

Beam	a/d	Experimental displacement (mm)	ATENA displacement (MPa)				Experimental/ATENA results			
			Model code	Euro code	Mander's Model	GRK Model	Model code	Euro code	Mander's Model	GRK Model
Dad1	1	3.7	3.7	3.74	3.79	3.79	1.00	0.99	0.98	0.98
Dad2	2	7.1	7.1	7.13	7.22	7.11	1.00	1.00	0.98	1.00
Dad3	3	3.95	4.03	4.03	4.03	4.03	0.98	0.98	0.98	0.98
Fad1	1	4.03	4.06	4.12	4.06	4.05	0.99	0.98	0.99	1.00
Fad2	2	5.87	5.94	5.94	5.9	5.9	0.99	0.99	0.99	0.99
Fad3	3	7.97	7.94	8.05	8.15	8.05	1.00	0.99	0.98	0.99
						Average	0.99	0.99	0.98	0.99

Table 6. Comparison of Experimental Displacement (mm) values at Centre Point corresponding to peak load with numerical displacement (mm) values.

Beam	a/d	Experimental displacement (mm)	ATENA displacement (MPa)				Experimental/ATENA results			
			Model code	Euro code	Mander's Model	GRK Model	Model code	Euro code	Mander's Model	GRK Model
Dad1	1	7.1	7.13	7.3	7.26	7.26	1.00	1.02	0.99	1.00
Dad2	2	13.3	13.44	13.37	13.26	13.35	1.01	0.99	0.99	1.01
Dad3	3	4.12	4.13	4.12	4.14	4.18	1.00	1.00	1.00	1.01
Fad1	1	8.21	8.43	8.4	8.44	8.39	1.03	1.00	1.00	0.99
Fad2	2	7.8	7.87	7.86	7.92	7.84	1.01	1.00	1.01	0.99
Fad3	3	9.65	9.89	9.78	10.1	9.72	1.02	0.99	1.03	0.96
						Average	1.01	1.00	1.01	0.99

concrete beams using different models predict similar behaviour which are on par with the experimental results.

5. The strains observed in numerical analysis using various models indicate that the high-strength reinforced concrete beams failed in shear, which was in good agreement with experimental shear failure patterns.

References

[1] Bahij S, Adekunle S, Al-Osta M, Ahmad S, Al-Dulaijan S, Rahman M. Numerical investigation of the shear behavior of reinforced ultra-high-performance concrete beams. Struct Concr. 2017;19(1):305-317.

Table 7. Comparison of experimental cracking shear strength (MPa) vs Numerical cracking shear strength (MPa).

Beam	a/d	Experimental Cracking shear strength (MPa)	ATENA results of cracking shear strength (MPa)				Experimental/ATENA results			
			Model code	Euro code	Mander's Model	GRK Model	Model code	Euro code	Mander's Model	GRK Model
Dad1	1	4.19	2.55	2.32	3.27	3.10	1.64	1.80	1.28	1.35
Dad2	2	2.72	1.31	1.02	1.51	1.46	2.08	2.66	1.80	1.87
Dad3	3	1.63	0.83	0.67	1.03	0.96	1.97	2.44	1.59	1.70
Fad1	1	5.37	3.58	3.37	4.35	4.20	1.50	1.60	1.24	1.28
Fad2	2	3.27	1.84	1.31	1.99	1.93	1.77	2.50	1.64	1.70
Fad3	3	2.18	1.08	0.84	1.30	1.23	2.01	2.58	1.68	1.77
						Average	1.83	2.26	1.54	1.61

[2] Kachouh N, El-Maaddawy T. Numerical analysis of concrete deep beams reinforced with glass fiber-reinforced polymer bars. Buildings. 2023;13(11):2767.

[3] Jiang CS, Liang GQ. Modeling shear strength of medium- to ultra-high-strength concrete beams with stirrups using SVR and genetic algorithm. Soft Comput. 2021;25(16):10661-10675.

[4] Hussein Amer Alhussein T, Abdul Samad Khudhair J. Experimental and numerical evaluation of shear strength of directly and indirectly loaded flanged recycled self-compacted reinforced concrete deep beams. J Eng. 2020;2020:3462010.

[5] Han D, Jung D. Numerical study on post-fire flexural and shear behavior of reinforced concrete beams. Protect Facil. 2025;2(3):186-192.

[6] Awad A, Tawfik M, Deifalla A, Ahmad M, Sabri Sabri MM, El-Said A. Effect of hybrid-fiber-reinforcement on the shear behavior of high-strength-concrete beams. Front Mater. 2023;9:1088554.

[7] Jude EO, Oh CH, Lee SC. Single web shear element model for shear strength of RC beams with stirrups. Int J Concr Struct Mater. 2018;12(1):27.

[8] Angelakos D, Bentz EC, Collins MP. Effect of concrete strength and minimum stirrups on shear strength of large members. ACI Struct J. 2001;98(3):291-300.

[9] Elzanaty AH, Nilson AH, Slate FO. Shear capacity of reinforced concrete beams using high-strength concrete. ACI Struct J. 1986;83(2):290-296.

[10] Bukhari IA, Ahmad S. Evaluation of shear strength of high-strength concrete beams without stirrups. Arab J Sci Eng. 2008;33(2):321.

[11] Desai SB. Influence of constituents of concrete on its tensile strength and shear strength. ACI Struct J. 2004;101(1):29-38.

[12] Ferguson PM. Some implications of recent diagonal tension tests. ACI Struct J. 1956;53(8):157-172.

[13] Bazant ZP, Kazemi MT. Size effect on diagonal shear failure of beams without stirrups. ACI Struct J. 1991;88(3):268-276.

[14] Kim JK, Park YD. Prediction of shear strength of reinforced concrete beams without web reinforcement. Farmington Hills (MI): American Concrete Institute.

[15] Ghannoum WM. Size effect on shear strength of reinforced concrete beams [dissertation]. Montreal: McGill University; 1998.

[16] Kani G. How safe are our large reinforced concrete beams? ACI Struct J. 1967;64(3):128-141.

[17] Tan KH, Cheng GH. Size effect on shear strength of deep beams: investigating

with strut-and-tie model. J Struct Eng. 2006;132(5):673-685.

[18] Bazant ZP, Kim JK. Size effect in shear failure of longitudinally reinforced beams. Farmington Hills (MI): American Concrete Institute; 1998.

[19] Collins MP, Kuchma D. How safe are our large, lightly reinforced concrete beams, slabs, and footings? ACI Struct J. 1999;96(4):482-490.

[20] Lubell A, Sherwood T, Bentz E, Collins M. Safe shear design of large wide beams. Concr Int. 2004;26(1):66-78.

[21] Muttoni A, Fernandez Ruiz M. Shear strength of members without transverse reinforcement as function of critical shear crack width. ACI Struct J. 2008;105(2):163-172.

[22] Kuo WW, Cheng TJ, Hwang SJ. Force transfer mechanism and shear strength of reinforced concrete beams. Eng Struct. 2010;32(6):1537-1546.

[23] Okamura H, Higai T. Proposed design equation for shear strength of reinforced concrete beams without web reinforcement. Proc Jpn Soc Civ Eng. 1980;300:131-141.

[24] Kannam P, Sarella VR. A study on validation of shear behaviour of steel fibrous SCC based on numerical modelling (ATENA). J Build Eng. 2018;19:69-79.

[25] Jaber HT, Sarsam KF, Muhammad BR. Literature review on size effect of shear reinforced concrete beams. AIP Conf Proc. 2023;2651(1).

[26] Srikanth MGRK, Rajesh KG, Giri S. Moment curvature of reinforced concrete beams using various confinement models and experimental validation. Asian J Civ Eng. 2007;8(3):247-265.

[27] Mander JB, Priestley MJN, Park R. Theoretical stress-strain model for confined concrete. J Struct Eng. 1988;114(8):1804-1826.

[28] Bureau of Indian Standards. IS 1489 (Part 1): Portland pozzolana cement—specification (Part 1: Fly ash based). New Delhi: BIS; 1991.

[29] Bureau of Indian Standards. IS 383: Coarse and fine aggregate for concrete—specification. New Delhi: BIS; 2016.

[30] Bureau of Indian Standards. IS 10262: Concrete mix proportioning—guidelines (second revision). New Delhi: BIS; 2019.

[31] Bazant ZP, Sun HH. Size effect in diagonal shear failure: influence of aggregate size and stirrups. ACI Mater J. 1987;84(4):259-272.

APPENDIX-A

The stress-Strain Curves of various diameters of steel are shown in Figs. 21-24.

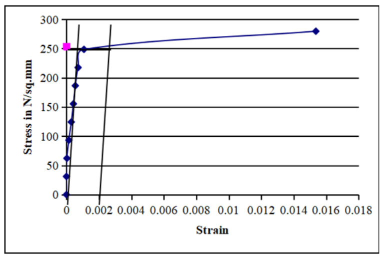

Fig. 21. Stress-Strain curve of 6mm diameter steel bar.

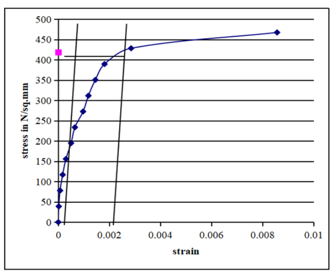

Fig. 22. Stress-Strain curve of 6mm diameter steel bar.

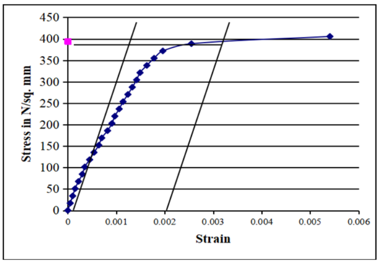

Fig. 23. Stress-Strain curve of 12mm diameter steel bar.

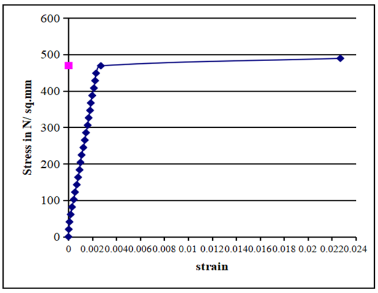

Fig. 24. Strains obtained using Numerical Analysis for Fad3 beam.

APPENDIX-B

The mesh size versus maximum shear force obtained on analyzing a plain cement concrete beam of grade 50 MPa were recorded in the Table A. The graph was plotted between mesh size (mm) on Y-axis and maximum shear force (kN) on X-axis and shown in Fig. 25. It can be clearly understood that as the mesh size becomes finer the maximum shear force value increased and becomes almost constant after reaching a mesh size of 5 mm. So, from this analysis of mesh sensitivity the mesh size was considered as 5 mm. The mesh size is not taken as 3 mm since computation time is almost double that of the mesh size 5 mm and result of maximum shear force (Peak Load) is same.

Table 8. Mesh size and corresponding Maximum Shear forces.

Mesh size (mm)	Maximum Shear Force (kN)
200	12.32
100	16.24
50	19.791
10	20.82
5	22.82
3	22.83

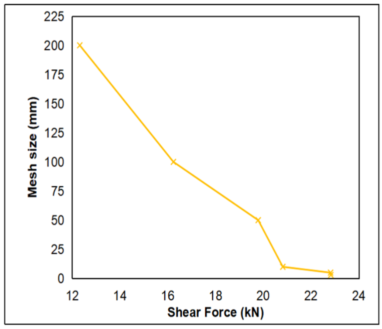

Fig. 25. Mesh size (mm) vs Shear Force (kN) for a PCC beam of strength 50 MPa.